Protein Science (1998), 7:1124–1135. Cambridge University Press. Printed in the USA.

The role of polar interactions in the molecular recognition of CD40L with its receptor CD40

JUSWINDER SINGH,[1] ELLEN GARBER,[1] HERMAN VAN VLIJMEN,[1] MICHAEL KARPUSAS,[1] YEN-MING HSU,[1] ZHONGLI ZHENG,[1] JAMES H. NAISMITH,[2] AND DAVID THOMAS[1]

[1]Biogen Inc., 14 Cambridge Center, Cambridge Massachusetts 02142
[2]Centre for Biomolecular Sciences, Purdie Building, The University, St. Andrews, KY169ST, Scotland, United Kingdon

(RECEIVED November 3, 1997; ACCEPTED January 30, 1998)

Abstract

CD40 Ligand (CD40L) is transiently expressed on the surface of T-cells and binds to CD40, which is expressed on the surface of B-cells. This binding event leads to the differentiation, proliferation, and isotype switching of the B-cells. The physiological importance of CD40L has been demonstrated by the fact that expression of defective CD40L protein causes an immunodeficiency state characterized by high IgM and low IgG serum levels, indicating faulty T-cell dependent B-cell activation. To understand the structural basis for CD40L/CD40 association, we have used a combination of molecular modeling, mutagenesis, and X-ray crystallography. The structure of the extracellular region of CD40L was determined by protein crystallography, while the CD40 receptor was built using homology modeling based upon a novel alignment of the TNF receptor superfamily, and using the X-ray structure of the TNF receptor as a template. The model shows that the interface of the complex is composed of charged residues, with CD40L presenting basic side chains (K143, R203, R207), and CD40 presenting acidic side chains (D84, E114, E117). These residues were studied experimentally through site-directed mutagenesis, and also theoretically using electrostatic calculations with the program Delphi. The mutagenesis data explored the role of the charged residues in both CD40L and CD40 by switching to Ala (K143A, R203A, R207A of CD40L, and E74A, D84A, E114A, E117A of CD40), charge reversal (K143E, R203E, R207E of CD40L, and D84R, E114R, E117R of CD40), mutation to a polar residue (K143N, R207N, R207Q of CD40L, and D84N, E117N of CD40), and for the basic side chains in CD40L, isosteric substitution to a hydrophobic side chain (R203M, R207M). All the charge-reversal mutants and the majority of the Met and Ala substitutions led to loss of binding, suggesting that charged interactions stabilize the complex. This was supported by the Delphi calculations which confirmed that the CD40/CD40L residue pairs E74-R203, D84-R207, and E117-R207 had a net stabilizing effect on the complex. However, the substitution of hydrophilic side chains at several of the positions was tolerated, which suggests that although charged interactions stabilize the complex, charge per se is not crucial at all positions. Finally, we compared the electrostatic surface of TNF/TNFR with CD40L/CD40 and have identified a set of polar interactions surrounded by a wall of hydrophobic residues that appear to be similar but inverted between the two complexes.

Keywords: CD40; CD40L; homology modeling; mutagenesis; TNF superfamily; X-ray crystallography

The co-stimulatory pair of molecules CD40 Ligand (CD40L) and its counter-receptor CD40, are involved in T- and B-cell cognate interactions that are crucial for B-cell activation. CD40L has also been implicated in T-cell activation by antigen presenting cells (APC; Grewal & Flavell, 1996a), which may be involved in the pathogenesis of certain diseases such as lupus (Mohan et al., 1995), arthritis (Durie et al., 1993), and Hodgkin's lymphoma (Gruss et al., 1994).

CD40L is a 33-kDa glycoprotein (Armitage et al., 1992; Graf et al., 1992; Lederman et al., 1992) that is transiently expressed on the surface of activated $CD4^+$ T-cells, and binds to its counter receptor, a 40-kDa glycoprotein CD40, which is expressed on the surface of a variety of APCs including B-cells and activated macrophages. The role of CD40L binding to CD40 in vivo has been studied using anti-CD40L monoclonal antibodies (mAbs; Durie et al., 1993) and CD40L knockout mice (Renshaw et al., 1994; Xu et al., 1994). The binding of CD40L to CD40 on B-cells results in immunoglobulin isotype switching, prevention of apoptosis, B-cell differentiation, and proliferation (Grewal & Flavell, 1996b). In both murine CD40L gene knockout experiments, and also in humans with mutations of CD40L that result in the X-linked primary immunodeficiency known as hyper IgM syndrome (HIGMS), there is an inability of B-cells to isotype switch from IgM to IgG, IgA and IgE production (Allen et al., 1993; Aruffo

Reprint requests to: Juswinder Singh, Biogen Inc., 14 Cambridge Center, Cambridge, Massachusetts 02142; e-mail: Juswinder_Singh@Biogen.com.

et al., 1993; DiSanto et al., 1993; Korthauer et al., 1993; Ramesh et al., 1993; Macchi et al., 1995). CD40L is a type II membrane protein, which, shortly after being cloned, was predicted to be a member of the TNF gene family (Farrah & Smith, 1992). This is a family of cytokines that includes TNF-α, TNF-β (LT-α), LT-β, CD30L, and FaS. The sequence similarity between CD40L and TNF-α and TNF-β is restricted to the receptor binding portion of the extracellular domains. Recently, the X-ray crystal structure of CD40L was determined (Karpusas et al., 1996). The structure showed that CD40L has the same topology as TNF-α (Eck & Sprang, 1989) and TNF-β (Eck et al., 1992), as predicted by Peitsch and Jongeneel (1993).

CD40 is a type I membrane protein that belongs to the nerve growth factor receptor gene family, which is characterized by cysteine-rich extracellular domains. This includes the 55 kDa TNF receptor (TNFR), 75 kDa TNF-receptor (TNFR2), and the low-affinity nerve growth factor receptor (p75). These proteins share little primary sequence similarity in their extracellular domains, apart from the cysteine pattern. The X-ray structure of the TNFR was first determined as part of a complex with TNF-β (Banner et al., 1993), and subsequently in the unliganded state at pH 7.5 (Naismith et al., 1995). The extracellular region of TNFR is composed of four domains of 44 amino acids. Three of these are structurally similar, and it was suggested by Banner et al. (1993) that these six cysteine, three disulfide domains, with the disulfide connectivity Cys1–Cys2, Cys3–Cys5, Cys4–Cys6 (Fig. 1), represent the repeating structural unit (the classical domain). A fourth domain could not be built due to disorder, but its sequence implied that it would have a different structure than the other three. The high-resolution structure of TNFR at low pH (Naismith et al., 1996) indeed showed a fourth domain, which was different in connectivity to the other three yet still contained six cysteines and three disulfide bridges.

As yet, no experimental structure of CD40 has been reported. An alternative approach has been to use the known X-ray structures of TNFR (Banner et al., 1993; Naismith et al., 1995) to build a homology model of CD40. The first model of CD40 was part of a complex with CD40L, which was built using the structure of the TNF-β/TNFR complex as a homology template and consisted of domains 2 and 3 (Bajorath et al., 1995a, 1995b). Recently, a more detailed model of CD40 has been built using the unliganded, pH 7.5, TNFR structure (hence called Model 1; Bajorath & Aruffo, 1997) and consists of domains 1 to 3. In the above models, the six cysteine, three disulfide bridge repeating unit was used as the template for homology modeling. These models of CD40 and CD40L have been used to identify regions involved in complexation using site-directed mutagenesis. The mutagenesis experiments have identified K143, Y145, Y146, R203, and Q220 in CD40L, and Y82, D84, N86, E74, and E117 of CD40 as important residues in binding (Bajorath et al., 1995a, 1995b; Bajorath & Aruffo, 1997). In addition, the models have been used to determine the positions that are mutated in HIGMS syndrome (Bajorath et al., 1995a, 1995b).

Recently, an alternative method for the homology modeling of CD40 has been proposed by Naismith and Sprang (1998), based upon a new way of aligning the TNF receptor superfamily. They argue that the basic repeating structural unit of TNFR is not the three disulfide bridge, 44 amino acid domain, but consists of a set of smaller modules (A1, B2, and D2) that are the building blocks for these domains. TNFR has the modular arrangement $A1x_0B2x_2A1x_2B2x_1A1x_2B2x_1A1x_2D2$ (where x_n is the spacing between the modules, with n being the number of residues). The four TNFR A1 modules have one disulfide bridge, C^1-C^2, and are 12 to 17 amino acids long with a consensus sequence C^1-x_2-G-x_1-A_r-x_{5-10}-C^2 (where C^y is Cys with y the disulfide connectivity and A_r is an aromatic residue). The three B2 modules are 21 to 24 amino acids long and contain two disulfide bridges, C^3 to C^6, with a consensus sequence C^3-x_2-C^4-x_{8-11}-C^5-T-x_{4-5}-N(D)-T-V-C^6. The combination of A1 and B2 modules, together with variation in the spacing between them (0 to 2 residues), is used to describe the structures of domains 1 to 3, and the first half of domain 4, of TNFR. The structures of six monomers of TNFR have been determined in different space groups, at different pH, in unliganded forms and in complex with TNF-β (Banner et al., 1993; Naismith et al., 1995, 1996). An analysis of the six independent crystallographic structures of TNFR confirmed that the modules rather than

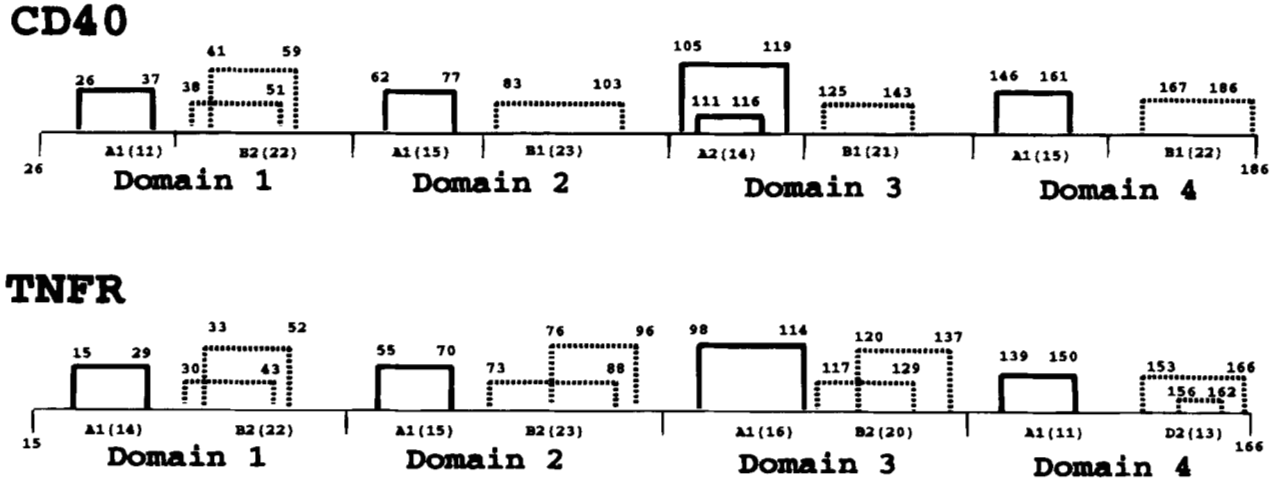

Fig. 1. Schematic representation of the modular arrangement and disulfide connectivity of $CD40_{26-186}$ and $TNFR_{15-166}$. Those cystines forming disulfide bridges have been numbered. The A modules are shown with a solid line and the B modules as a dashed line. The size of each module is shown in parenthesis.

the domains are structurally rigid (Naismith & Sprang, 1996). It also showed that the connections between the modules are flexible and allow the protein considerable freedom to deform and maximize protein–protein interactions. This modular approach has been used to describe the structures of other members of the TNFR superfamily (Naismith & Sprang, 1998). To make this possible, it was necessary to rationalize stretches of sequence where there is an excess of cysteines or a paucity of cysteines. Naismith and Sprang (1998) suggested that the structure of these regions can be described using two new modules called A2 and B1 modules, which are variants in structure of the A1 and B2 modules described above. The A2 and B1 modules have the same size ranges as their A1 and B2 counterparts, have similar signature sequences, but have either an additional disulfide (A2) or a missing disulfide (B1), which have been shown to be easily accommodated into the structures (Naismith & Sprang, 1998). The D2 module, which has recently been identified in the fourth domain of TNFR, does not appear to be present in other members of the superfamily. It should be noted that the D2 module that we define here is termed C2 elsewhere (Naismith et al., 1996), and is referred to as D2 here to avoid confusion with the disulfide bridge nomenclature used above.

We have generated a three-dimensional structure of CD40L and CD40 using the X-ray structure of the receptor binding extracellular portion of CD40L (Karpusas et al., 1995), together with a model of CD40 based upon the modular approach of Naismith and Sprang (1998; hence called Model 2). Model 2 was used to identify interaction sites between the receptor and ligand, several of which were subsequently tested using site-directed mutagenesis. Model 2, together with experimental data, point to the importance of charged residues in the recognition between CD40L and its receptor CD40.

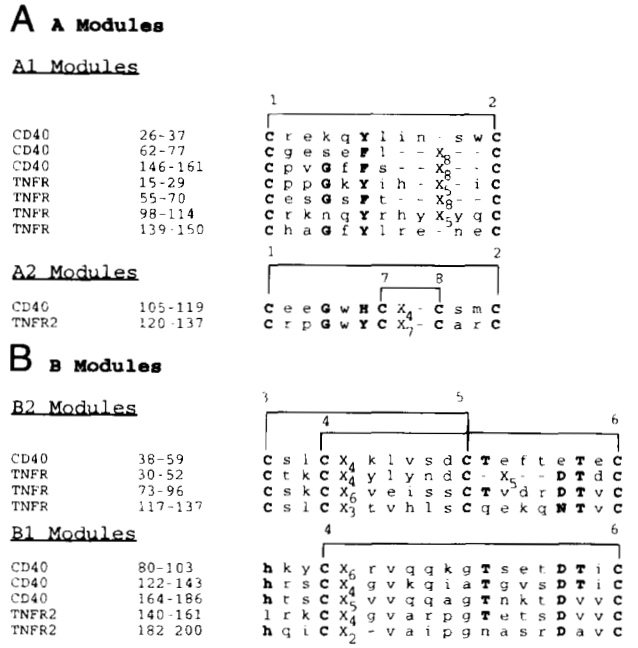

Fig. 2. Alignment of the A and B modules of TNFR, TNFR2, and CD40, which is based upon that published by Naismith and Sprang (1998). The disulfide connectivity of the modules is shown by a solid line. **A:** A modules. **B:** B modules.

Results

Modular definition of CD40

Based upon the consensus sequences defined for A and B modules in TNFR (Fig. 2), we assigned the following modular arrangement (Fig. 3) to CD40 from residue 26–186 ($CD40_{26-186}$): $A1x_0B2x_2A1x_2B1x_1A2x_2B1x_2A1x_2B1$.

All three of the CD40 A1 modules ($CD40_{26-37}$, $CD40_{62-77}$, $CD40_{146-161}$) are consistent with the TNFR A1 consensus C^1-x_2-G-x_1-A_r-x_{4-10}-C^2, with the disulfide connectivity C^1-C^2, although Gly is not absolutely conserved in CD40 ($CD40_{26-37}$, $CD40_{62-77}$). However, it should be noted that Gly is not present in one of the four A1 modules ($TNFR_{98-114}$) of TNFR. The predicted A2 ($CD40_{105-119}$) module of CD40 has the motif C^1-x_2-G-x_1-H-C^7-x_4-C^8-x_2-C^2, which is similar to the TNFR A1 consensus shown above, but has an additional disulfide bridge C^7-C^8, and is predicted by us to have a similar structure to the A1 modules. As will be shown below, the additional disulfide within the A2 module is accommodated with minimal disruption to the structure of the A1 template used to model the module. Banner et al. (1993) first suggested such an encapsulated disulfide bridge between Cys104 and Cys112 for the 75kD form of the TNF receptor (TNFR2).

The single B2 domain of CD40 ($CD40_{38-59}$) has the motif C^3-x_2-C^4-x_9-C^5-T-x_3-E-T-E-C^6, and is similar to the TNFR consensus sequence C^3-x_2-C^4-x_{8-11}-C^5-T-x_{3-4}-N(D)-T-V-C^6, with the disulfide connectivities C^3-C^5 and C^4-C^6. The CD40 B1 modules are predicted to have a similar structure to the B2 module, and have the consensus sequence H-x_2-C^4-x_{10-12}-T-x_3-D-T-I-C^6, which is similar to that of the B2 consensus of TNFR, but is missing the C^3-C^5 disulfide bridge.

CD40L and CD40 structure

The X-ray crystal structure of the extracellular fragment of $CD40L_{116-261}$ has been described in detail elsewhere (Karpusas et al., 1996). It exists as a trimer and has the same topology as TNF-α and TNF-β. However, there are considerable differences in several loop regions, including those predicted to be involved in CD40 binding.

Our model of human CD40 (Model 2) consists of residues 26 to 143 (denoted $CD40_{26-143}$). The sequence alignment used to generate Model 2 is shown in Figure 3. As with previously published models (Bajorath et al., 1995a, 1995b; Bajorath & Aruffo, 1997), we based the structural alignment of CD40 on CD40L on the crystal structure of TNF Receptor with TNF-β. Our assumption is that the high degree of structural similarity between CD40L and TNF-β (Karpusas et al., 1995) extends to the way that their receptors are structurally aligned. To align CD40L with CD40, our first step was to align the crystal structure of CD40L with the TNF-β/TNFR structure, using the strands A-H of TNF-J as structural equivalences (Karpusas et al., 1995). This created an alignment of CD40L with the TNF/TNFR complex. The TNFR was then used as a template to model build CD40. Our model consists of the first three of the four homologous domains. Although the structure of domain 4 ($CD40_{145-186}$) was originally built in Model 2, we have omitted this from our model due to uncertainty in the orientation of domain 3 with respect to domain 4. This was based on the observation that the orientation of domain 3 with respect to domain 4 differs between the low and high pH form of TNFR (Naismith et al., 1996).

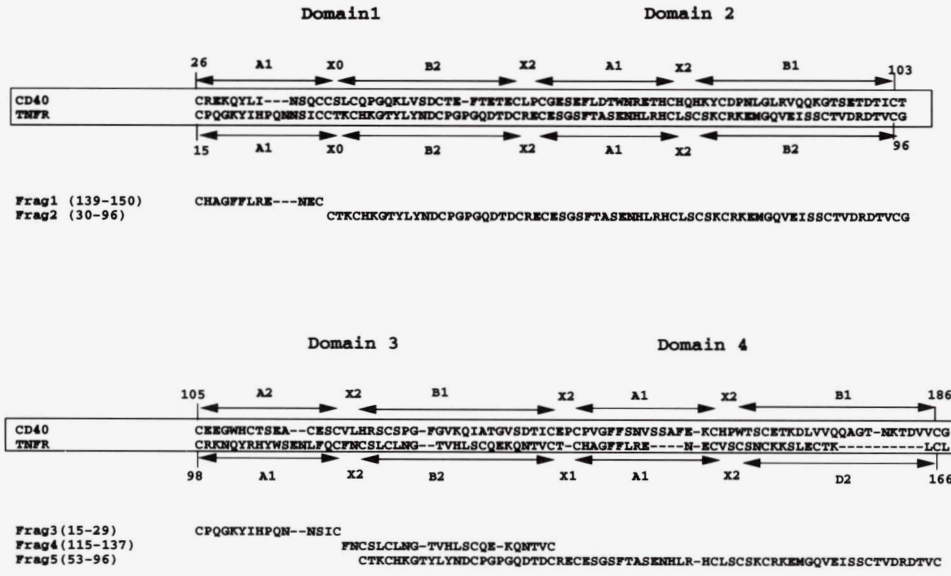

Fig. 3. Sequence alignment of $CD40_{26-166}$ with TNFR for Model 1 and Model 2. The alignment as defined by Bajorath and Aruffo (1997) is shown in a box, below which is the alignment for Model 2 based upon fragments (Frag1–Frag5) of TNFR.

The overlay of the energy minimized model of CD40 with the X-ray structure of TNFR is shown in Figure 4. The overall conformation of CD40 is very similar to that of TNFR; the largest difference is the conformation of the A2 module of domain 3 of $CD40_{105-119}$ and the A1 module of $TNFR_{98-114}$. The root-mean-square deviation (RMSD) of the C-α atoms of CD40 before and after minimization was only 0.48 Å. The residues at the interface mostly affected by the minimization were R73 (mass weighted RMSD of side-chain atoms = 3.5 Å), H76 (3.3 Å), Q79 (2.4 Å), N86 (1.3 Å), and A115 (3.1 Å). The minimizations generally did not cause any side-chain rotamer changes except for R73, in which the $\chi 3$ dihedral angle changes from trans to gauche. The movement of A115 was associated with a uniform displacement of the local protein backbone. A significant change in $\chi 1$ angle was seen

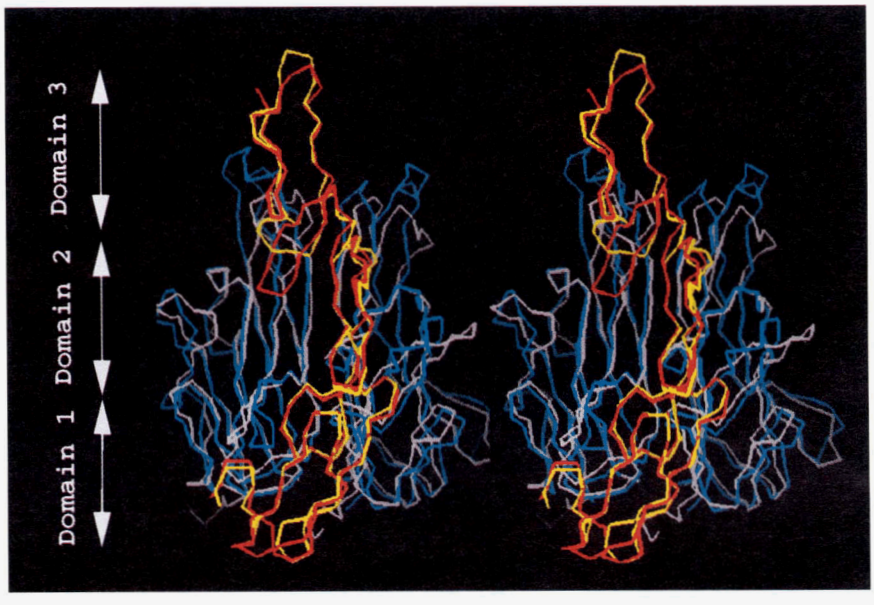

Fig. 4. Overlay of the C-α trace of domains 1 to 3 of the minimized CD40 (Model 2) complexed with the X-ray crystal structure of CD40L (Karpusas et al., 1996) with domains 1 to 3 of the X-ray structure of TNFR complexed with TNF-β (Banner et al., 1993). The color scheme is as follows: CD40 yellow, TNFR red, TNF cyan, and CD40L white. Domains 1 to 3 have been labeled.

for Y82 (−89° to −44°), which did not have any steric overlap with CD40L, but changed its conformation to better interact with K143 in CD40L.

To assess the stereochemical quality of the model, we used the program PROCHECK (Laskowski et al., 1996) to compare the geometry of residues in the CD40 model with the stereochemical parameters observed in well-resolved, high-resolution protein structures. Analysis of the ϕ, φ dihedral angles of the CD40 showed that 75% of the residues are within the most favored regions of the Ramachandran plot, which is similar to the 78% in the TNFR X-ray structure of Banner et al. (1993). There are three residues in disallowed regions in CD40 (S35, T55, C125), which compares to two residues in TNFR (G18, N101).

The three domains of CD40 form an elongated molecule with their disulfides organized in a ladder-like arrangement. Domain 1 consists of an A1 and B2 module joined with no intervening residues. These modules extend over the base of the bell-shaped CD40L trimer, and although close to the N-terminus of CD40L, they do not form any interactions with the ligand. In contrast, the A1 and B1 modules of domain 2 and the A2 module of domain 3 ($CD40_{105-119}$) form extensive interactions with the interface of two CD40L subunits. The remaining modules of CD40 do not form contacts with CD40L.

The CD40 model differs from TNFR in having stretches where there is a paucity of cystines (B1 modules) and an excess of cystines (A2 modules). How does the CD40 model accommodate these differences? The B1 modules, $CD40_{80-103}$ and $CD40_{122-143}$, differ from the B2 modules in TNFR, upon which they were built, by having one instead of two disulfide bridges. As predicted by Naismith and Sprang (1998), the disulfide is structurally replaced by a side-chain/main-chain hydrogen-bonding interaction between the strands. More specifically, this is between the side chain of H80 and the backbone of T96 of $CD40_{80-103}$ and between the side chain of H122 and the backbone of T136 of $CD40_{122-143}$. The one A2 module of $CD40_{105-119}$ differs from the A1 modules of TNFR in having an additional disulfide bridge between Cys111–Cys116. By using the domain 1 A1 module ($TNFR_{15-29}$) of TNFR as a template for the A2 module of CD40 (because it is of the same size), and replacing I21 and N26, the disulfide is accommodated with minimal alterations in the main-chain conformation.

CD40L/CD40 interface

The surface area buried upon complexation of CD40L and CD40 in our Model 2 is 834 Å^2 [accessible surfaces calculated using the method described by Banner et al. (1993) with CHARMM, nonhydrogen atoms only], which is slightly smaller than that reported for Model 1 [931–1,123 Å^2; Bajorath et al. (1995b)], and also somewhat lower than that seen in the TNF/TNFR complex (1,130 A^2; Banner et al., 1993).

The residue–residue contacts (distance <5 Å between any heavy atom) between CD40L and CD40 were: S65, E66$^{\$}$, T70, R73, E74, H76, C77, H78, Q79, K81, Y82, D84$^{\$}$, N86, T112, E114, A115, and E117$^{\$}$ from CD40 and I127, S128, E129, E142, K143, G144, Y145, Y146, C178, S185$^{\#}$, Q186$^{\#}$, A187$^{\#}$, R200, F201, R203$^{\#}$, R207$^{\#\$}$, C218, Q220, S248, H249, G250, T251, and G252 from CD40L (where # refers to CD40L residues from the second symmetry related subunit, and $ refers to contacts between acidic and basic residues greater than 5 Å and less than 7 Å). All residue contacts involve domains 2 and 3 of CD40 with two of the subunits of the CD40L trimer. Contacts between basic and acidic residues are shown in boldface, and include E74-R200 and E74-R203. Three additional contacts between oppositely charged residues (E66-K143, D84-R207, and E117-R207) have separation distances somewhat larger than 5 Å.

The interface of the complex is polar. The electrostatic potential on the solvent accessible surface of CD40L, as calculated by Delphi (Nicholls & Honig, 1991) and visualized by GRASP (Nicholls et al., 1991) is shown in Figure 5. The regions of positive potential are shown in blue, and the regions of negative potential in red. The CD40L surface has three regions of positive potential in contact with the CD40 structure. These regions are formed by the positively charged side chains R203, R207, and K143. This suggests that these residues could have significant electrostatic interactions with the receptor. We have quantified, using Delphi, the complementarity of the electrostatic potentials by calculating the stabilization of the positive charge of K143, R203, and R207 by residues across the CD40L/CD40 interface. For R203 and R207, the stabilization energies due to the full CD40 protein are relatively similar (−2.1 and −2.2 kcal/mol), while that of K143 is roughly half in magnitude (−1.1 kcal/mol). The results show that K143 is stabilized mainly by E66 (−0.8 kcal/mol), and R203 by E74 (−1.9 kcal/mol). R207 is stabilized by D84 (−0.9 kcal/mol) and E117 (−1.0 kcal/mol).

For the four charged pairs E66-K143, E74-R203, D84-R207, and E117-R207, we calculated the electrostatic contribution to CD40/CD40L complex stabilization (see Materials and methods) in terms of the total electrostatic stabilization $\Delta\Delta G_{el}$ and its three constituent terms $\Delta\Delta G_{solv}$, $\Delta\Delta G_{protein}$, and $\Delta\Delta G_{bridge}$ (all free energy values in kcal/mol).

One of the four pairs (E66-K143) has a net electrostatic destabilizing effect on the complex, which is caused by a relatively large desolvation penalty (4.1 kcal/mol), which is not compensated by $\Delta\Delta G_{protein}$ or $\Delta\Delta G_{bridge}$. Of the three stabilizing residue pairs, E74-R203 is the strongest salt bridge in the model, based upon the relatively close distance (3.2 Å), the relatively large desolvation energy (4.8 kcal/mol) and the total electrostatic stabilization $\Delta\Delta G_{el}$ (−2.4 kcal/mol)

A similar but inverted set of polar interactions that are common to CD40L/CD40 and TNF/TNFR

The TNF surface is dominated by a region of negative electrostatic potential which is in an equivalent position to the positive electrostatic potential arising from R207 in CD40L (Fig. 5A). Closer inspection of the site in TNF shows that unlike CD40L, which has R207 in this region, TNF has Q118 in a similar location (Fig. 5C). In CD40, a region of negative potential, arising from D84 and E117 (Fig. 5b), is nearby the R207 on the CD40L surface. In contrast to CD40L, where the positive potential is contributed by the ligand, in the TNF/TNFR complex, R77 exists on the receptor surface at a structurally equivalent position to that of D84 in CD40.

R207 in CD40L and Q118 in TNF are similar in that they both occur at the interface of their respective trimers and are both surrounded by a wall of hydrophobic residues (Fig. 6A,B). R207 is surrounded by I190, F253, I204, and T251, while Q118 is surrounded by V158, L130, Y96, T163, and V80. These hydrophobic residues are predicted to increase the strength of the electrostatic interactions between the polar residues in the complex by a reduction in solvent screening.

Although the negative potential opposite R77 is largely due to E100 and D152, the electrostatic stabilization of R77 (−4.1 kcal/

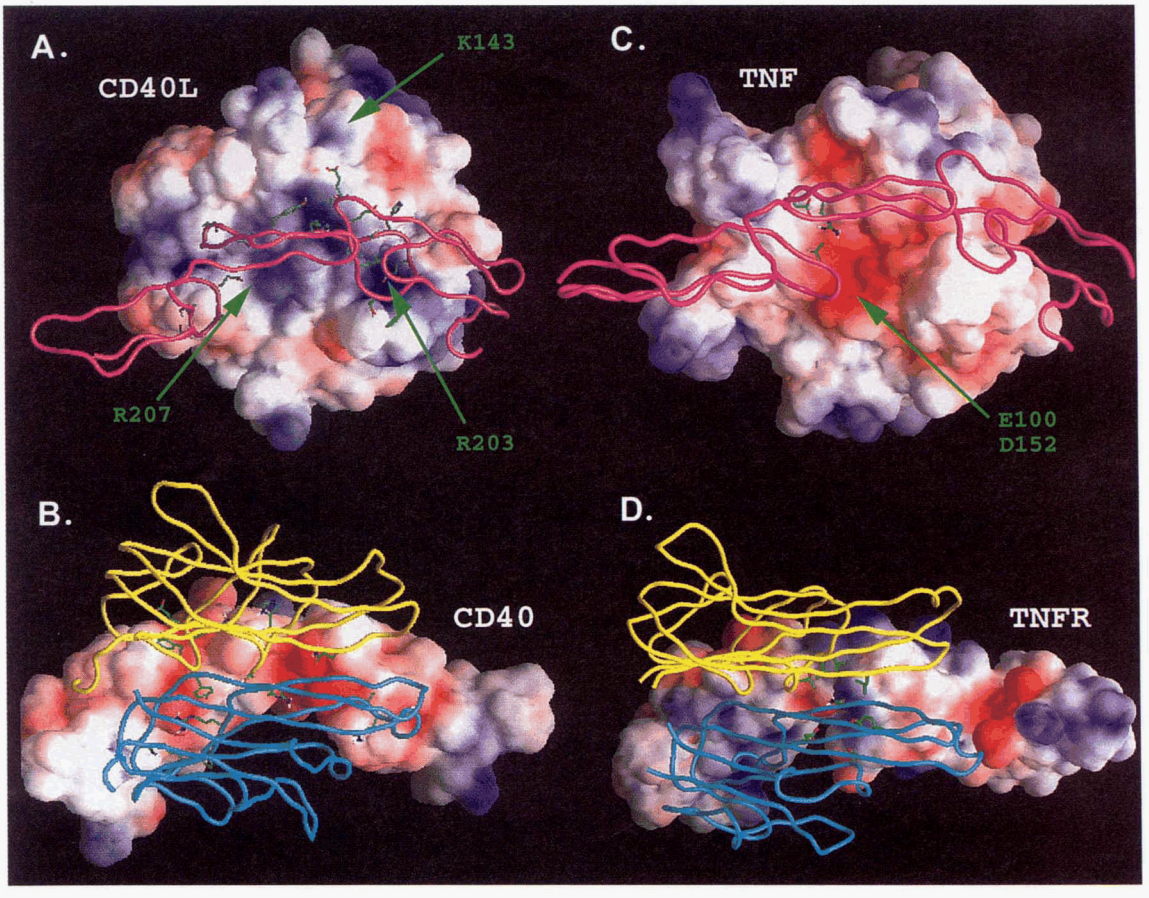

Fig. 5. GRASP representation of electrostatic potential of the 3D structures of (**A**) CD40L, (**B**) CD40, (**C**) TNF-β, and (**D**) TNFR at their respective solvent accessible surfaces. The negative potential was colored red and displayed at -3 kT level, the positive potential was colored blue and displayed at $+3$ kT level ($T = 298$ K). The C-α trace of of the corresponding complex partners are also displayed.

mol) is due mainly to a hydrogen bonding interaction with the side-chain carbonyl of Q118 (-3.3 kcal/mol).

Mutagenesis of CD40-Ig and CD40L

We explored the importance of several of the polar residues at the CD40L/CD40 interface using site-directed mutagenesis. These included K143, R203, and R207 of CD40L, and E74, D84, E114, and E117 of the extracellular portion of CD40 fused to human-IgG1 Fc (CD40-Ig; see Materials and methods). Each of the positions was mutated to explore the effect of charge reversal, switching to a neutral side chain, changing to Ala, and switching to a hydrophobic side chain.

We transiently expressed CD40L in its full-length membrane-bound form. We verified that all mutant CD40Ls were expressed and indirectly assessed their structural integrity by immunoprecipitation of detergent lysates from metabolically labeled cells with polyclonal antibodies directed against synthetic peptides corresponding to the N- and C-terminal portion of CD40L (Hsu et al., 1997), or with the anti-CD40L mAb 5c8 (Fig. 7), which can block CD40/CD40L-mediated signaling (Lederman et al., 1992; Yellin et al., 1994). Cell surface expression of CD40L of selected mutants positive for 5c8 binding was verified by FACS staining of intact transfected cells with 5c8 (data not shown). All were expressed as assayed by binding to the N- and C-terminal–specific antisera (Table 1). We cannot definitively rule out that the mutant CD40L's structural integrity has been compromised, but immunoprecipitation by antibodies directed against distinct epitopes suggests that they retain their native 3D structure. We assessed CD40L/CD40 binding by examining the ability of metabolically labeled mutant CD40Ls from detergent extracts of transfected cells to be immunoprecipitated by purified wild-type (wt) CD40-Ig (prepared from a stable CHO cell line, see Hsu et al., 1997). A summary of our results for CD40L mutants is shown in Table 1. All of the mutant CD40L proteins that showed limited binding to 5c8 also showed reduced or complete loss of binding to CD40-Ig. There exists the possibility that these mutants (K143E, K143A, R207E, and R207M) could be either affecting the structure of the CD40L or an important binding site epitope, common to both CD40-Ig and anti-CD40L mAb 5c8. Our results with K143A are consistent with the work of Bajorath et al. (1995a), who show that three of their five anti-CD40L mAbs show reduced binding to mutant CD40L K143A. In addition, our results show that, although K143A and K143E do not bind, the K143R mutation is tolerated. Similarly, although R207E results in complete loss of binding to 5c8, R207A is tolerated.

The wtCD40L showed normal binding to CD40-Ig. It appears that the polar character at residues at positions K143, R203, and R207 are crucial for binding to CD40. The mutation of the above

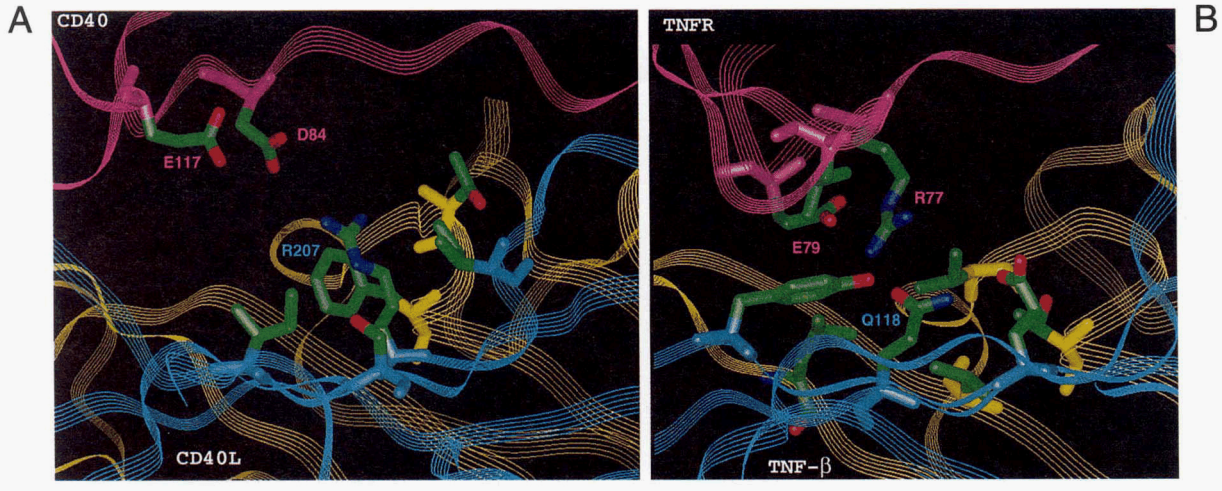

Fig. 6. Plot of contact sites of (**A**) R207 of CD40L in the CD40L/CD40 complex and (**B**) Q118 of TNF-β in the TNF/TNFR complex. The receptor and ligand backbones are shown in a ribbon representation (CD40 and TNFR, purple ribbon; CD40L and TNF-β; yellow and cyan ribbon denoting two chains of the trimer).

three positions to Ala leads to loss of binding of CD40L to CD40. Because the mutation of the basic side chains to Ala results in the substitution of a large side chain for a smaller side chain, we felt it important to mutate the positions to a hydrophobic side chain that was more similar in size. Once again, mutation of each of the above positions to Met resulted in loss of binding. If the basic side chains were replaced with acidic side chains (K143E, R203E, R207E), there was complete loss of binding. However, both K143E and R207E also affected 5c8 binding, which raises the possibility that these mutations could be effecting the structure of the CD40L. Interestingly, mutation of R207 to Asn or Gln was tolerated, suggesting that charge at this position is not crucial. Finally, we explored whether the type of basic side chain at the above three positions had any effect on binding. The mutations K143R and R207K still bound to CD40 like wtCD40L, but R203K led to complete loss of binding.

For mutants of CD40, Fc-fusion proteins were prepared for analysis of their expression and functional activities. The expression of Fc-fusion proteins was verified by immunoprecipitation using protein A beads followed by western blotting with anti-CD40 mAb, B-B20 (Fig. 8). To assay the functional activity of these CD40 mutants, these Fc-fusion proteins were used to immunoprecipitate cells. Table 2 shows the results of CD40 mutations of four acidic residues. It should be pointed out that none of the mutations caused a loss of expression of these CD40-Fc fusion proteins. In

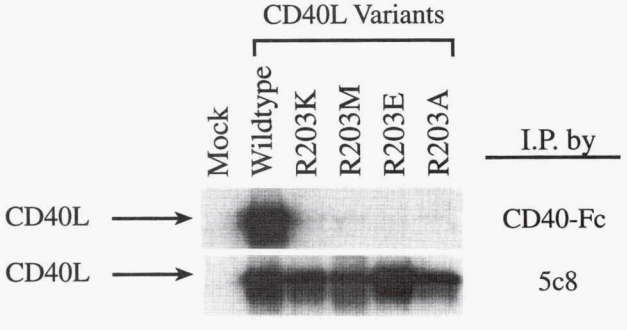

Fig. 7. Functional analysis of Arg203 mutants of CD40L. COS cells were transfected with mock plasmid or plasmid containing cDNAS encoding the wild-type and mutants of CD40L, metabolically labeled 48 h post-transfection, lysed, and immunoprecipitated with anti-CD40L mAB, 5c8 (lower panel) or with CD40-Fc fusion protein (upper panel) and analyzed by a 10–20% SDS-PAGE gradient under reducing conditions.

Table 1. *Expression and functional analysis of CD40L variants*[a]

CD40L variant	5c8 immpt	CD40Fc immpt	α-N-terminus	α-C-terminus
Wild type	+	+	+	+
R203A	+	−	+	+
R203E	+	−	+	+
R203M	+	−	+	+
R203K	+	−	+	+
R207A	+	±	+	+
R207E	−	−	+	+
R207K	+	+	+	+
R207N	+	+	+	+
R207Q	+	+	+	+
R207M	±	±	+	+
K143A	±	±	+	+
K143E	±	−	+	+
K143N	+	−	+	+
K143R	+	+	+	+

[a]COS cells were transfected with a mock plasmid or plasmid containing cDNA encoding the wild-type or mutant of CD40 ligand, metabolically labeled at 48 h after transfection, lysed, and immunoprecipitated with anti-CD40L mAb, 5c8 (column 1), CD40-Fc fusion protein (column 2), a rabbit antiserum that specifically recognizes the N-terminal (column 3) or C-terminal (column 4) portion of CD40L, and analyzed by a 10–20% gradient SDS-PAGE under reducing conditions. For comparison, "+" represents signal that is comparable to the wild type; "±" for signal significantly less, nevertheless detectable, than the wild type; and "−" reflects undetectable signal.

terms of functionality, mutation of the acidic residues (either Asp or Glu) to Ala invariably resulted in a loss of reactivity toward CD40L, suggesting the charge of the residues may play an important role in ligand–receptor interactions. On the other hand, substitution of the acidic residues with basic side chains appears detrimental for residues D84 and E117, but not for E114. Interestingly, neither D84N nor E117N mutation affect the interaction of CD40 to its ligand, indicating that while changing to a basic residue abolishes the function, substitution with a neutral but hydrophilic residue is tolerated.

Table 2. *Expression and functional analysis of CD40 variants*[a]

CD40-FC variants	Western blot (BB20)	CD40L immpt
Wild type	+	+
E74A	+	−
D84A	+	−
D84E	+	±
D84N	+	+
D84R	+	−
E114A	+	±
E114R	+	+
E117A	+	−
E117D	+	+
E117N	+	+
E117R	+	−

[a]COS cells were transfected with cDNA encoding the wild type or variants of CD40-Fc fusion protein and harvested at three days post-transfection. The expression of CD40-Fc protein was verified using murine anti-human CD40 mAb, BB20 (column 1). The functional activity of CD40-Fc variants was evaluated by their abilities to immunoprecipitate the metabolically labeled CD40L that was produced in the transiently transfected COS cells (column 2). For comparison, "+" represents signal that is comparable to the wild type; "±" for signal significantly less, nevertheless detectable, than the wild type; and "−" reflects undetectable signal.

Discussion

The binding of CD40L on activated T-cells to CD40 on B-cells plays a crucial role in the activation and proliferation of B-cells and activation of T-cells. There exists impressive data in rodents (Larsen et al., 1996) and more recently in primates (Kirk et al., 1997), that blockade of this pathway could be therapeutically useful. Here we have used a combination of molecular modeling, X-ray crystallography, and site-directed mutagenesis to generate a detailed picture of the CD40L/CD40 complex. This information is useful both in understanding the molecular basis for CD40L/CD40 complexation and also for the design of antagonists to inhibit their association.

There exist two principal differences between our structure–function studies of CD40L/CD40 and those published previously (Bajorath et al., 1995a, 1995b). The first is our use of the X-ray crystal structure of CD40L, which, although it has the same topology as TNF-α and TNF-β, has considerable differences in several loops including those predicted to be involved in binding to CD40 (Karpusas et al., 1995). The second principal difference is the novel alignment of CD40 with TNFR, and our treatment of loop regions in the CD40 model. Our CD40 alignment (Model 2) differs from that previously published (Model 1; Bajorath et al., 1995b; Bajorath & Aruffo, 1997) for the second half of domain 1, approximately three-quarters of domain 3, and all of domain 4. However, the alignments are the same for domain 2, which forms most of the contact surface with CD40L. Therefore, although there are significant differences between the two sequence alignments overall, there are clearly similarities in the 3D models for the definition of the CD40 interface with CD40L. One consequence of our alignment has been that we have modeled the insertions/deletions of CD40 by using the TNFR structure directly, by taking modules of similar size and module type. In contrast, Model 1's insertions/deletions have been model built using conformational search methods (Bruccoleri & Novotny, 1992).

The mutagenesis data reported to date on CD40L/CD40 have been limited to Ala scanning. Our data confirm the work of Bajorath et al. (1995a, 1995b) that mutation to Ala of the positions K143 and R203 of CD40L and D84, E114, and E117 of CD40 results in loss of binding of the complex. The work described here has extended the mutational analysis of the CD40L/CD40 complex to explore the effect of charge reversal, mutation to a neutral side chain, as well as to isosteric substitution (substitution to Met)

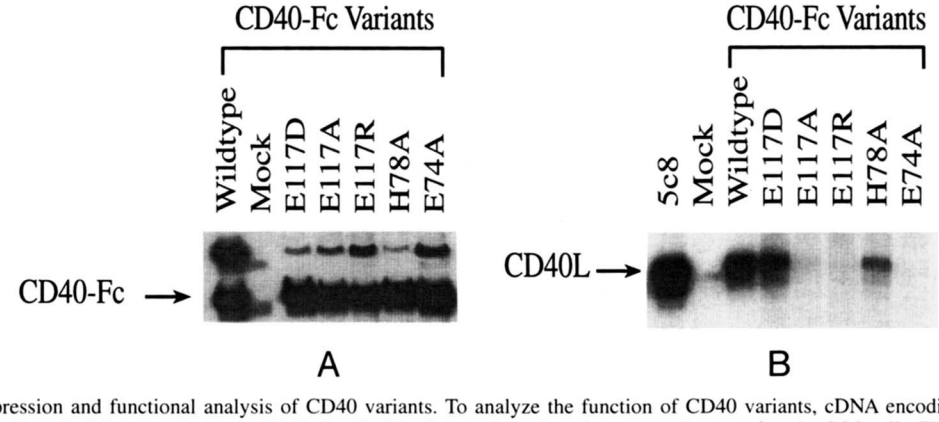

Fig. 8. Expression and functional analysis of CD40 variants. To analyze the function of CD40 variants, cDNA encoding the extracellular domains of wild-type and mutant CD40, fused with a human IgFc domain, was used to transfect the COS cells. The media from the transfected COS cells were harvested and used to immunoprecipitate the metabolically labeled CD40L (**A**). To verify the expression of CD40-Fc variants, COS cells were metabolically labeled 48 h post-transfection. The medium was harvested, fractionated by protein A beads, and analyzed by a 10–20% SDS-PAGE gradient under reducing conditions (**B**).

of specific charged residues predicted to be at the interface. Our data show that mutation of positions K143, R203, and R207 of CD40L and E74, D84, and E117 of CD40 to a residue of opposite charge leads to loss of binding of the complex. One exception is the E114R mutation, which binds like wild type, suggesting that the E114A mutation that led to loss of binding, may have affected the structure of the complex. In addition to charge reversal, mutation R203 and R207 of CD40L to Met also leads to loss of binding of the complex. This mutagenesis data, together with our electrostatic calculations using the CD40L/CD40 structure, suggest that these residues are involved in ion pairs that are stabilizing the complex. Our data are in accordance with that of Xu et al. (1997), who have studied the general importance of ion pairs in stabilizing protein–protein interfaces. They show through the use of continuum electrostatic calculations on X-ray structures of protein complexes that salt bridges can significantly stabilize protein interfaces. The importance of hydrophilic pair interactions in stabilizing protein–protein complexes has also been studied by Xu et al. (1997). They found a positive correlation between free energy of complex formation and the number of hydrophilic bridges across an interface in an analysis of known three-dimensional structures of protein complexes. Our data suggest that with CD40L/CD40, although charged interactions stabilize the complex, they can be replaced with hydrophilic interactions and retain binding. The mutagenesis data show that certain positions can tolerate replacement of charged residues with polar side chains on both CD40L and CD40 (D84N and E114N of CD40 and R207N and R207Q of CD40L). It will be important to determine how many of the above-charged residues can be replaced by polar residues and still maintain binding of the CD40L/CD40 complex.

In summary, we have examined experimentally and theoretically the molecular interface between CD40 and CD40L and found that charge–charge interactions play an important role in binding. This provides new insight into the recognition of another member of the TNF superfamily.

Materials and methods

CD40 model building

The $CD40_{26-186}$ was built using the X-ray structure of the 55 kDa TNF-β receptor solved by Banner et al. (1993) (hence called TNFR) using the homology modeling module of InsightII (version 2.3.5; Biosym Technologies). Unlike an earlier model of the CD40 (Model 1; Bajorath et al., 1995b; Bajorath & Aruffo, 1997), which was based upon the six cystine, three disulfide bridge repeating unit as the template for homology modeling (see Fig. 1), our model (Model 2) was based upon using the A and B modules of TNFR as defined by Naismith and Sprang (1998) as the template for CD40. They define the modular arrangement of CD40, based upon comparison to A and B consensus sequences in TNFR, as $A1x_0B2x_2A1x_2B1x_1A2x_2B1x_2A1x_2B1$.

Unlike previously published models of CD40 (Bajorath et al., 1995a, 1995b; Bajorath & Aruffo, 1997), we first modified our TNFR template by rearranging several of the modules within the structure. This was necessary because the most suitable modules of TNFR to act as a template to model-build CD40 were not always from the corresponding domain. The CD40 model was constructed from five fragments of TNFR (see Fig. 2). For example, the first module of $CD40_{26-37}$, which lies within domain 1, was not built using the first module of $TNFR_{15-29}$ from domain 1, but instead by using a module from domain 4 of $TNFR_{139-150}$ (fragment 1) because it was of a similar type and size. To rearrange the TNFR modules we used the structural equivalences based upon the work of Naismith and Sprang (1998). This work shows that A and B modules are structurally more conserved than the domains. Fragment 1 was fitted onto $TNFR_{15-29}$ using the following structural equivalences: $TNFR_{15-21}$:$TNFR_{139-145}$ (in which $TNFR_{x-y}$:$TNFR_{a-b}$ define the Ca positions of the TNFR fragments being superposed, with x-y defining the stretch of the target structure to be fitted onto and a-b defining the stretch of the template being transformed to be used in the model building of CD40) and $TNFR_{29}$:$TNFR_{150}$. The $CD40_{38-104}$ $B2x_2A1x_2B1$ motif was built using the corresponding stretch, $B2x_2A1x_2B2$, of $TNFR_{30-97}$ (fragment 2) and, therefore, no transformation was necessary. The $CD40_{105-119}$ A2 domain was built using the A1 domain of $TNFR_{15-29}$ (fragment 3) because it was of the same length. The fragment was transformed onto the TNFR template by fitting onto the $TNFR_{98-114}$ using the following equivalences $TNFR_{15-21}$:$TNFR_{98-104}$ and $TNFR_{29}$:$TNFR_{114}$. The $CD40_{120-143}$ B1 domain was built using the corresponding stretch of $TNFR_{115-137}$ (fragment 4), which involved a single residue insertion. The $CD40_{144-186}$ $A1x_2B1$ motif was built using the $TNFR_{53-96}$ (fragment 5). To orient fragment 5 onto the TNFR template, the preceding B2 domain $TNFR_{30-52}$ was used to fit onto $TNFR_{117-137}$ using the following equivalences $TNFR_{30-34}$:$TNFR_{117-121}$, $TNFR_{38-44}$:$TNFR_{124-130}$, and $TNFR_{49-52}$:$TNFR_{134-137}$. The transformation matrix obtained was then applied to fragment 5.

The structure of the extracellular region of CD40L was determined by X-ray crystallography (Brookhaven code: 1ALY) as described by Karpusas et al. (1995) to a resolution of 2.0 Å with an R-factor of 21.8%. Because the CD40 model was based upon the TNFR structure in the TNF-β/TNFR complex, we oriented the CD40L structure with respect to CD40 by superimposing CD40L onto TNF using the C-α positions of the strands A–H (Fig. 4 of Karpusas et al., 1995) as structural equivalences.

To remove unfavorable steric contacts from the CD40 model, we energy minimized the CD40 structure in the presence of the fixed crystal structure of CD40L. The program CHARMM (Brooks et al., 1983) was used, using the all-hydrogen parameter set 22 (MacKerell et al., 1998), with a distance dependent dielectric constant of two times the atom separation distance. We first did 1000 steps of steepest descent minimization with mass-weighted harmonic positional constraints of 1 kcal/(mol A^2) on all atoms of CD40. This minimization was followed by another 1,000 steepest descent and 5,000 Adopted-Basis Newton Raphson steps with constraints of 0.1 kcal/(mol A^2) on the C-α atoms of CD40 only, to avoid significant deviations of the CD40 backbone from the TNFR structure.

Electrostatic analysis

We analyzed various electrostatic interactions in the CD40L/CD40 and TNF/TNFR complexes using the program Delphi (Nicholls & Honig, 1991). The program solves the linearized Poisson–Boltzmann equation to obtain the electrostatic potential in and around the protein, while taking the presence of solvent into account as a high dielectric continuum. The protein internal dielectric constant was set to 4 in all calculations, and the solvent dielectric constant was 80. The salt concentration was set to 145 mM, which corresponds to physiological ionic strength. Atomic

charges and radii were assigned according to the CHARMM all-hydrogen parameter set 22 (MacKerell et al., 1998).

For several basic residues (Arg, Lys) in CD40L and TNF, which are located at the protein–protein interface in the CD40L/CD40 and TNF/TNFR complexes, we calculated the electrostatic stabilization of the positive charge (of the basic residue) due to residues of the neighboring protein. This was done by removing all atomic charges from both proteins in the complex, except the charges corresponding to the residue(s) that are analyzed for their stabilizing effects. We then used Delphi to calculate the electrostatic potential, assign charges to the basic residue, and calculate the electrostatic energy of the basic residue in the potential. By taking the difference between the energies of the protonated and unprotonated basic residue, we get a quantitative measure of the electrostatic stabilization. For example, to calculate the stabilizing effect of Glu74 (CD40) on Arg203 (CD40L), we did the following: (1) calculate the electrostatic potential in the CD40L/CD40 complex with Delphi, where only Glu74 atoms have assigned charges; (2) assign charges to Arg203 and calculate its electrostatic energy by multiplying the atomic point charges by the corresponding potentials. Do this for protonated and unprotonated Arg203; (3) subtract the energy of the unprotonated Arg203 from the protonated Arg203.

In addition, we calculated the electrostatic contribution to CD40/CD40L complex stabilization of the following residue pairs (CD40 residue–CD40L residue): Glu66–Lys143, Glu74–Arg203, Asp84–Arg207, and Glu117–Arg207. We used the method described by Hendsch and Tidor (1994) and Xu et al. (1997). The method consists of calculating the difference in total electrostatic free energy between the residue pair in the complex and in the separate proteins. The total electrostatic free energy difference $\Delta\Delta G_{el}$ was calculated by adding three terms: the solvation free energy difference $\Delta\Delta G_{solv}$ of the residues, the difference in electrostatic interactions with residues other than the residue pair ($\Delta\Delta G_{protein}$), and the direct electrostatic interaction energy $\Delta\Delta G_{bridge}$ between the residues of the pair (Hendsch & Tidor, 1994).

The electrostatic potential calculations with Delphi were done using an initial grid with a spacing of 0.75 Å that contained the receptor (CD40 or TNFR) and two of the three chains of the ligand trimer (CD40L or TNF) with which it interacts. The initial grid calculation was followed by focusing calculations with a spacing of 0.25 Å. The electrostatic potentials generated by Delphi were displayed using GRASP (Nicholls et al., 1991).

Production of CD40-Ig

The huCD40 gene was cloned from a human tonsil cell-derived lgt10 cDNA expression library screened using probes homologous to the 5′ and 3′ ends of huCD40. The open reading frame encoding CD40 was subcloned from the phage DNA into a unique NotI site in a pUC-derived vector. Sequence analysis was performed to confirm the identity of the CD40 sequence (Stamenkovic et al., 1989). To produce a soluble CD40-Ig fusion protein, the first two amino acids of the trans-membrane domain were mutagenized to introduce a SalI restriction site to fuse the entire CD40 extracellular domain to a SalI restriction site introduced into a modified cDNA copy of the human IgG1 Fc (hinge starting at Kabat residue 232, CH2, and CH3 domains). Sequence analysis confirmed the mutagenesis. A CMV-IE promotor-driven expression vector was constructed by subcloning a NotI-SalI CD40 extracellular domain fragment and a SalI-NotI fragment IgG1 Fc fragment into a unique NotI site in the expression vector. The vector was transfected into COS7 cells. Transfected cells secreted CD40-Ig fusion protein were recognized by either CD40-specific or human IgG Fc-specific antibodies and that could immunoprecipitate CD40L. An adenovirus major late promotor-driven expression vector containing a dihydrofolate reductase selectable marker was constructed and transfected into CHO cells to produced stable cell lines. Clones were selected in 200 nM methotrexate and positives were identified by screening supernatants by ELISA or on Western blots using human IgG Fc-specific antibody. The best producer was adapted to suspension culture for scaleup. Sequence analysis of the purified CD40-Ig fusion protein indicated that its N-terminus was identical to that of native CD40.

Transient expression of CD40L mutants in COS cells

Mutants of CD40L were made by unique site elimination mutagenesis using a Pharmacia kit, following the manufacturer's recommended protocol. The CD40L target pUC-derived plasmid contained the full-length wild-type CD40L cDNA (its open reading frame flanked by minimal 5′ and 3′ untranslated sequences). If a desired mutation did not produce a restriction site change, a silent mutation producing a restriction site change was introduced into an adjacent codon to facilitate identification of mutant clones following mutagenesis. The desired mutations were confirmed by DNA sequencing. Wild-type or mutant CD40L cDNAs were subcloned into an expression vector into which heterologous gene expression is driven by a CMV-IE promotor and an SV40 transcriptional termination and polyA addition site. Presence of the introduced restriction site change was reconfirmed in the expression vector for each CD40L mutant. The expression vector contains an SV40 origin for amplification in COS cells. COS7 cells were electroporated with super-coiled plasmid. Empty vector lacking the CD40L gene was used as a negative control, and a vector containing wild-type CD40L was used as a positive control in all experiments. Transfected cells were metabolically labeled overnight with ^{35}S-translabel before being harvested at 3 days post-transfection. Labeled cells were lysed in buffer containing 1% NP4 and 0.5% deoxycholate. The lysates were clarified by centrifugation (10 min, 10,000 × *g*) and pre-cleared with protein A-Sepharose beads and anti-CD40L–specific antibodies (humanized mAB 5c8, or N- or C-terminal CD40L anti-peptide rabbit polyclonal antisera) or 5 mg of CD40-Ig for 90 min at 4 °C. Immune complexes collected on protein A beads were washed three times with lysis buffer and treated with Laemmli sample buffer before being resolved by SDS polyacrylamide gel electrophoresis. Immunoprecipitation of CD40L mutants was compared to that of wild-type CD40L.

Transient expression of CD40-Ig mutants in COS cells

Mutants of CD40-Ig were made by unique site elimination mutagenesis using Pharmacia kit following the manufacturer's recommended protocol. The target pUC-derived plasmid contained the NotI-SalI fragment carrying the CD40 extracellular domain from the previously described CD40-Ig expression vector. If a desired mutation did not produce a restriction site change, a silent mutation producing a restriction site change was introduced into an adjacent codon to facilitate identification of mutant clones following mutagenesis. The desired mutations were confirmed by DNA sequencing. Wild-type or mutant CD40-Ig cDNAs were reconstructed by subcloning into an expression vector in which heterologous gene expression is driven by a CMV-IE promotor and an SV40 tran-

scriptional termination and polyA addition site. Presence of the introduced restriction site change was reconfirmed in the expression vector for each CD40-Ig mutant. The expression vector contains an SV40 origin for amplification in COS cells. COS7 cells were electroporated with supercoiled plasmid. Empty vector lacking the CD40-Ig gene was used as a negative control and a vector containing wild-type CD40-Ig was used as a positive control in all experiments. To confirm CD40-Ig expression, transfected cells were metabolically labeled overnight with ^{35}S-translabel before being harvested at three days post-transfection. Labeled cell supernatants were clarified by centrifugation (10 min, 14,000 × *g*) and were immunoprecipitated with protein A-Sepharose beads. Immune complexes collected on protein A beads were washed three times with lysis buffer and treated with Laemmli sample buffer before being resolved by SDS-polyacrylamide gel electrophoresis. Alternatively, supernatants from unlabeled cells were immunoprecipitated with protein A-Sepharose, and SDS-polyacrylamide gel-resolved immune complexes analyzed by Western blot analysis using the CD40-specific mAb BB-20. Both methods produced equivalent results with respect to CD40-Ig expression. To assay CD40L binding by mutant CD40-Ig proteins, lysates from ^{35}S-labeled wild-type CD40L-expressing transfected COS cells were immunoprecipitated with protein A-Sepharose and supernatants from unlabeled CD40-Ig–expressing transfected COS cells. Immune complexes collected on protein A beads were washed three times with lysis buffer and treated with Laemmli sample buffer before being resolved by SDS-polyacrylamide gel electrophoresis. Immunoprecipitation of CD40L by CD40-Ig mutants was compared to that of wild-type CD40-Ig.

Acknowledgments

We would like to thank Barbara Ehrenfels and Evelyn Madigan, and the Biogen sequencing group for their excellent technical assistance. We would also like to thank Steve Adams and Gurmit Kaur for their help and encouragement. The coordinates of the CD40L X-ray structure have been deposited in the Brookhaven Data Bank (pdbcode 1ALY), and the coordinates of the CD40/CD40L complex are available upon request.

References

Allen RC, Armitage RJ, Conley ME, Rosenblatt H, Jenkins NA, Copeland NG, Bedell MA, Edelhoff S, Disteche CM, Simoneaux DK, Fanslow WC, Belmont J, Spriggs MK. 1993. CD40 ligand gene defects responsible for X-linked hyper-IgM syndrome. *Science 259*:990–993.

Armitage RJ, Fanslow WC, Strockbine L, Sato TA, Clifford KN, Macduff BM, Anderson DM, Gimpel SD, Davis-Smith T, Maliszewski CR, Clark EA, Smith CA, Grabstein KH, Cosman D, Spriggs MK. 1992. Molecular and biological characterization of a murine ligand for CD40. *Nature 357*:80–82.

Aruffo A, Farrington M, Hollenbaugh D, Li X, Milatovich A, Nonoyama S, Bajorath J, Grosmaire LS, Stenkamp R, Neubauer M, Roberts RL, Noelle RJ, Ledbetter JA, Francke U, Ochs HD. 1993. The CD40 ligand, gp39, is defective in activated T-cells from patients with X-linked Hyper-IgM syndrome. *Cell 72*:291–300.

Bajorath J, Aruffo A. 1997. Construction and analysis of a detailed 3D model of the ligand binding domain of the human B cell receptor CD40. *Proteins Struct Funct Genet 27*:59–70.

Bajorath J, Chalupny NJ, Marken JS, Siadak AW, Skonier J, Gordon M, Hollenbaugh D, Noelle RJ, Ochs HD, Aruffo A. 1995a. Identification of residues on CD40 and its ligand which are critical for the receptor-ligand interaction. *Biochemistry 34*:1833–1844.

Bajorath J, Marken JS, Chalupny NJ, Spoon TL, Siadak AW, Gordon M, Noelle RJ, Hollenbaugh D, Aruffo A. 1995b. Analysis of gp39/CD40 interactions using molecular models and site-directed mutagenesis. *Biochemistry 34*:9884–9892.

Banner DW, D'Arcy A, Janes W, Gentz R, Schoenfeld HJ, Broger C, Loetscher H, Lesslauer W. 1993. Crystal structure of the soluble human 55kd TNF receptor-human TNF-b complex: Implications for TNF receptor activation. *Cell 73*:431–445.

Brooks BR, Bruccoleri RE, Olafson BD, States DJ, Swaminathan S, Karplus M. 1983. CHARMM: A program for macromolecular energy minimization and dynamics calculations. *J Comp Chem 4*:187–217.

Bruccoleri RE, Novotny J. 1992. Antibody modeling using the conformational search program CONGEN. *Immunomethods 1*:96–106.

DiSanto JP, Bonnefoy JY, Gauchat JF, Fischer A, De Saint Basile G. 1993. CD40 ligand mutations in X-linked immunodeficiency with hyper IgM. *Nature 361*:541–543.

Durie FH, Fava RA, Foy TM, Aruffo A, Ledbetter JA, Noelle RJ. 1993. Prevention of collagen-induced arthritis with an antibody to gp39, the ligand for CD40. *Science 261*:1328–1330.

Eck MJ, Sprang SR. 1989. The structure of TNF-a at 26A resolution. *J Biol Chem 264*:17595–17605.

Eck MJ, Ultsch M, Rinderknecht E, de Vos AM, Sprang SR. 1992. Lymphotoxin-b, a novel member of the TNF family that forms a heteromeric complex with lymphotoxin on the cell surface. *J Biol Chem 267*:2119–2122.

Farrah T, Smith CA. 1992. Emerging cytokine family. *Nature 358*:26.

Graf D, Korthauer U, Mages HW, Senger G, Kroczek RA. 1992. Cloning of TRAP, a ligand for CD40 on human T-cells. *Eur J Immunol 22*:3191–3194.

Grewal IS, Flavell RA. 1996a. A central role of CD40 ligand in the regulation of CD4+ T-cell responses. *Immunol Today 17*:410–414.

Grewal IS, Flavell RA. 1996b. The role of CD40 ligand in costimulation and T-cell activation. *Immunol Rev 153*:85–106.

Gruss, HJ, Hirschstein D, Wright B, Ulrich D, Caligiuri MA, Barcos M, Strockbine L, Armitage RJ, Dower SK. 1994. Expression and function of CD40 on Hodgkin and Reed-Sternberg cells and the possible relevance for Hodgkins disease. *Blood 84*:2305–2314.

Hendsch ZS, Tidor B. 1994. Do salt bridges stabilize proteins? A continuum electrostatic analysis. *Protein Sci 3*:211–226.

Hsu YM, Lucci J, Su L, Ehrenfels B, Garber E, Thomas D. 1997. Heteromultimeric complexes of CD40 ligand are present on the cell surface of human T lymphocytes. *J Biol Chem 272*:911–915.

Karpusas M, Hsu Y, Wang J, Thompson J, Lederman S, Chess L, Thomas D. 1995. The crystal structure of a TNF-like extracellular fragment of human CD40 ligand at 20 Å resolution. *Structure 3*:1031–1039.

Korthauer U, Graf D, Mages HW, Briere F, Padayachee M, Malcom S, Ugazio AG, Notarangelo LD, Levinsky RJ, Kroczek RA. 1993. Defective expression of T-cell CD40 ligand causes X-linked immunodeficiency with hyper-IgM. *Nature 361*:539–541.

Kirk AD, Harlan DM, Armstrong NN, Davis TA, Dong Y, Gray GS, Hong X, Thomas D, Fechner JH Jr, Knechtle SJ. 1997. CTLA4-Ig and anti-CD40 ligand prevent renal allograft rejection in primates. *Proc Natl Acad Sci USA 94*:8789–8794.

Larsen CP, Elwood ET, Alexander DZ, Ritchie SC, Hendrix R, Tucker-Burden C, Cho HR, Aruffo A, Hollenbaugh D, Linsley PS, Winn KJ, Pearson TC. 1996. Long-term acceptance of skin and cardiac allografts after blocking CD40 and CD28 pathways. *Nature 381*:434–438.

Laskowski RA, MacArthur MW, Moss DS, Thornton JM. 1996. PROCHECK: A program to check the stereochemical quality of protein structures. *J Appl Crystallogr 26*:283–291.

Lederman S, Yellin MJ, Krichevsky A, Belko J, Lee JJ, Chess L. 1992. Identification of a novel surface protein on activated CD40$^+$ T cells that induces contact-dependent B cell differentiation help. *J Exp Med 175*:1091–1101.

Macchi P, Villa A, Strina D, Sacco MG, Morali F, Brugnoni D, Giliani S, Mantuano E, Fasth A, Anderson B, Zegers BJM, Cavagni G, Reznick I, Levy J, Zan-Bar I, Porat Y, Airo P, Plebani A, Vezzoni P, Notarangelo LD. 1995. Characterization of nine novel mutations in the CD40 ligand gene in patients with X-linked hyper IgM syndrome of various ancestry. *Am J Hum Genet 56*:898–906.

MacKerell AD Jr, Bashford D, Bellot M, Dunbrack R Jr, Field MJ, Fischer S, Gao J, Guo H, Ha S, Joseph D, Kuchnir L, Kuczera K, Lau FTK, Mattos C, Michnick S, Ngo T, Nguyen DT, Prodhom B, Roux B, Schlenkrich M, Smith JC, Stote R, Straub J, Wiorkiewicz-Kuczera M, Karplus M. 1998. All-hydrogen empirical potential for molecular modeling and dynamics studies of proteins using CHARMM22 force field. *J Am Chem Soc*. In press.

Mohan C, Shi Y, Laman JD, Datta SK. 1995. Interaction between CD40 and its ligand gp39 in the development of murine nephritis. *J Immunol 154*:1470–1480.

Naismith JH, Devine TQ, Brandhuber BJ, Sprang SR. 1995. Crystallographic evidence for dimerization of unliganded tumor necrosis factor. *J Biol Chem 270*:13303–13307.

Naismith JH, Devine TQ, Brandhuber BJ, Sprang SR. 1996. Structures of the extracellular domains of the type I tumour necrosis factor receptor. *Structure 4*:1251–01262.

Naismith JH, Sprang SR. 1996. Tumor necrosis factor receptor superfamily. *J Inflamm 47*:1–7.

Naismith JH, Sprang SR. 1998. Moving to a modular system: The TNF receptor superfamily. *Trends Biosci 23*:74–78.

Nicholls A, Honig B. 1991. A rapid finite difference algorithm, utilizing successive over relaxation to solve the Poisson-Boltzman equation. *J Comp Chem 12*:435–445.

Nicholls A, Sharp KA, Honig B. 1991. Protein folding and association: Insights from the interfacial and thermodynamic properties of hydrocarbons. *Proteins Struct Funct Genet 11*:281–296.

Peitsch MC, Jongeneel CV. 1993. A 3-D model for the CD40 ligand predicts that it is a compact trimer similar to the tumor necrosis factors. *Int Immunol 5*:233–238.

Ramesh N, Fuleihan R, Ramesh V, Lederman S, Yellin MJ, Sharma S, Chess L, Rosen FS, Geha RS. 1993. Novel deletions in the ligand for CD40 in X-linked immunoglobulin deficiency with normal or elevated IgM (HIGMX-1). *Int Immunol 5*:769–774.

Renshaw BR, Fanslow WC, Armitage RJ, Cambell KA, Liggit D, Wright B, Davison BL, Maliszewski CR. 1994. Humoral immune responses in CD40 ligand-deficient mice. *J Exp Med 180*:1889–1900.

Roy M, Aruffo A, Ledbetter J, Linsley P, Kehry M, Noelle R. 1995. Studies on the interdependence of gp39 and B7 expression and function during antigen-specific immune responses. *Eur J Immunol 25*:596–603.

Spriggs MK, Armitage RJ, Strockbine L, Clifford KN, Macduff BM, Sato T, Maliszewski CR, Fanslow WC. 1992. Recombinant human CD40 ligand stimulates B-cell proliferation and immunoglobulin E secretion. *J Exp Med 176*:1543–1550.

Stamenkovic I, Clark EA, Seed B. 1989. A B-lymphocyte activation molecule related to the nerve growth factor receptor and induced by cytokines in carcinomas. *EMBO J 8*:1403–1410.

Xu D, Lin SL, Nussinov R. 1997. Protein binding versus protein folding: The role of hydrophilic bridges in protein associations. *J Mol Biol 265*: 68–84.

Xu J, Foy TM, Laman JD, Elliot EA, Dunn JJ, Waldschmidt TJ, Elsemore J, Noelle RJ, Flavell RA. 1994. Mice deficient for the CD40 ligand. *Immunity 1*:423–431.

Yellin MJ, Sippel K, Inghirami G, Covey LR, Lee JJ, Sinning J, Clark EA, Chess L, Lederman S. 1994. CD40 molecules induce down-modulation and endocytosis of T cell surface T cell-B cell activating molecule/CD40-L. Potential role in regulating helper effector function. *J Immunol 152*:598–608.